to zero and the estimation error for this profile is equal to 1°C over all the lossy material under investigation.

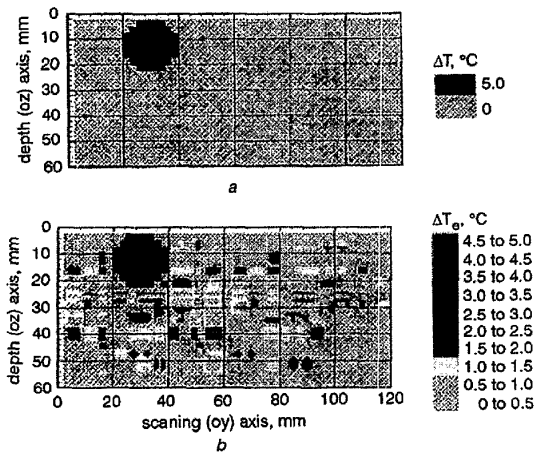

Fig. 2 *Experimental and estimated temperature difference-depth profiles*

a Experimental temperature difference-depth profile (sphere at $T = T_0 + \Delta T$), $\Delta T = 5$°C placed in water at $T_0 = 20$°C and $Z = 12.5$mm
b Estimated temperature difference-depth profile by Kalman algorithm from measured radiometric signals

Results: We show in Fig. 2*a* the experimental temperature difference-depth profile, composed of water at an ambient temperature of $T_0 = 20$°C, in which a sphere at temperature $T_0 + \Delta T$ ($\Delta T = 5$°C) is placed at $Z = 12.5$mm. Fig. 2*b* shows the estimated temperature distribution obtained by the Kalman algorithm. We note that from the estimated temperature-depth profile from the experimental surface measured with the radiometer receiver (sensitivity 0.1°C, for delay time $\tau = 0$), and by applying eqn. 2, we can locate the temperature gradients in the lossy material.

Conclusion: The results obtained by applying the proposed Kalman algorithm prove the practical feasibility of a new thermal inversion approach involving the determination of temperature gradients in biological tissues. Our method has enabled us to realise a non-invasive microwave technique for controlling the temperature-depth profile within biological tissues and to provide a quantitative guidance for the treatment of cancerous tumours. This new approach has also been made possible due to the miniaturisation of the experimental bench.

Acknowledgments: This work was supported by the CNCPRST of Morocco (Réseau d'Electronique et de Microondes et de leurs applications REMA).

21 December 1999
Electronics Letters Online No: 20000311
DOI: 10.1049/el:20000311

S. Bri and L. Bellarbi (*Laboratoire LGE, ENSET, BP 6207, Rabat Instituts, Morocco*)

E-mail: lbellarbi@hotmail.com

M. Habibi (*Laboratoire LAMO, Université Ibn Tofail, Faculté des Sciences, Kénitra, Morocco*)

M. ELKadiri (*Laboratoire LEC, EMI, Agdal, Rabat, Morocco*)

A. Mamouni (*Laboratoire NAMO, IEMN-DHS, UMR CNRS 9929, Université de Lille, France*)

S. Bri: Also with Laboratoire LAMO, Université Ibn Tofail, Faculté des Sciences, Kénitra, Morocco

References

1 BOCQUET, B., VAN DE VELDE, J.C., MAMOUNI, A., LEROY, Y., GIAUX, G., DELANNOY, J., and DELVALEE, D.: 'Microwave radiometric imaging at 3GHz for the exploration of breast tumors', *IEEE Trans.*, 1990, **MTT-38**, (6), pp. 791–793

2 MIZHUSHINA, S., SHIMIZU, T., SUZUKI, K., KINOMURA, M., OHBA, H., and SUGIURA, T.: 'Retrieval of temperature-depth profiles in biological objects from multifrequency microwave radiometric data', *J. Electromag. Waves Applic.*, 1993, **7**, (11), pp. 1515–1548

3 BOCQUET, B., AÏT-ABDELMALEK, R., and LEROY, Y.: 'Deconvolution and wiener filtering of short range radiometric images', *Electron. Lett.*, 1993, **29**, (18), pp. 1628–1629

4 BELLARBI, L., ELKADIRI, M., LEROY, Y., and MAMOUNI, A.: 'Temperature retrieval in lossy material by microwave correlation radiometry', *Electron. Lett.*, 1994, **30**, (8), pp. 658–660

5 RIDAOUI, K., BOCQUET, B., MAMOUNI, A., and LEROY, Y.: 'Computation of microwave radiometric weighting functions for industrial and medical applications'. Proc. PIERS'97, Hong Kong, January 1997

6 BELLARBI, L.: 'Radiométrie microonde par corrélation, reconnaissance des gradients thermiques dans un milieu dissipatif: Applications médicales'. PhD, 1994, Université Mohamed V, EMI, Rabat, Morocco

7 EMMANUEL, C.: 'A parallel implementation of Kalman filtering on transputers', *L'Onde Electrique*, 1989, **69**, (3), pp. 39–50

8 BELLARBI, L., ELKADIRI, M., MAMOUNI, A., and LEROY, Y.: 'Modélisation des signaux radiométriques. Application à la Radiométrie Microonde'. Proc. 1st Journées Franco-Marocaines sur les Microondes et leurs Applications (JFMA'96), EMI, Rabat, Morocco, 28–30 May 1996

Low-power variable length decoder considering successive codewords

Sung-won Lee and In-Cheol Park

A low-power variable length decoder which exploits the statistics of successive codewords is presented. The decoder employs a small look-up table working as a fixed cache to reduce the number of activations of a variable length code detector, where most power is consumed. The power simulation results estimated with Powermill show a 35% average reduction in energy compared with that of the previous low-power scheme.

Introduction: The variable length code (VLC) is effective at minimising the average code length, and is thus widely used in many multimedia compression systems such as MPEG and H.263 to relax the bit rate and storage requirements. To realise a high throughput decoder, Lei and Sun proposed a VLC decoder (VLD) that can decode one codeword per cycle [1]. The VLD consists of two major blocks, a VLC detector and a set of look-up tables (LUTs). The VLC detector consists of an accumulator and a barrel shifter. The output of the barrel shifter is fed into the LUTs which convert a codeword to a corresponding symbol. To determine the position of the next codeword, the size of the decoded codeword is fed back to the accumulator which controls the barrel shifter.

Although the VLD proposed by Lei and Sun is useful for achieving high throughput, it is not optimised for low-power applications, the number of which is increasing rapidly owing to the rapid development of portable multimedia systems. Therefore, a considerable amount of effort has been devoted to low-power applications, which can be classified into two categories. First, much research has been focused on reducing the power of the LUTs, as reported in [1], in which a considerable amount of power is consumed. A number of schemes such as prefix predecoding [2] and table partitioning [3] have been presented which have led to a significant reduction in LUT power. Secondly, attempts have been made to reduce the power of the VLC detector, and several schemes proposed such as VLC detector sizing [3] and barrel shifter optimisation [4]. In all of these approaches it is assumed that a codeword is independent of others, and no consideration is made about the relationship between codewords.

In this Letter, we propose a new low-power VLC decoder in which the characteristics of successive codewords are considered.

Observation: We have investigated the statistics of input codewords and the power dissipation of VLDs designed by using the low-power techniques explained above. The power dissipation was simulated for various design configurations obtained by changing the output size of the VLC detector from 8 bits to 12 and then 16 bits, and changing the input size of the LUTs from 2 bits to 15 bits. For the MPEG2 DCT AC coefficients, the power consumption was estimated using Powermill and a 0.35μm cell

library. The investigation leads to two major observations for the design of low-power VLDs.

First, the power consumption of a VLC detector is much larger than that of LUTs, 5 times, 10 times and 20 times larger for an 8 bit, 12 bit, and 16 bit VLC detector, respectively. This result implies that the number of activations of a VLC detector should be minimised, and that LUT partitioning does not have a significant effect on reducing power as the dominant proportion of power is consumed in the VLC detector.

The second observation is that short codewords are arranged successively with high probability. In experimental results, the average probability that a short codeword is followed by another short codeword is as high as 0.8. As the basic principle of variable length coding is to assign short codewords to frequent input symbols, the observation seems to be natural. Since the output size of a VLC detector is usually enough to cover two short codewords, this observation can be used in reducing the activation level of a VLC detector by permitting one activation for two short codewords. This is very different from previous schemes in which a VLC detector is activated for every codeword.

Proposed VLD: The proposed scheme involves the introduction of a small-sized LUT called a cache next to the traditional LUT storing short codewords. The cache is accessed when a short codeword is detected in the LUT to eliminate the activation of a VLC detector which consumes a large amount of power.

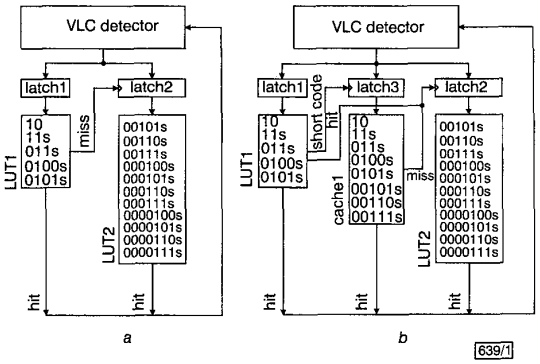

Fig. 1 *VLD architecture*
a Conventional VLD [3]
b Proposed VLD

The proposed scheme is shown in Fig. 1*b*, which works as follows. The VLC aligned in the VLC detector is decoded in the first LUT, LUT1. The most frequent codewords such as '10', '11s', and '011s' are located in LUT1. Once a symbol is found in LUT1, meaning that the codeword is short, a new codeword is searched in the next cycle at the cache, cache1, without invoking the VLC detector to shift the VLC. In the next cycle, latch3 is clocked to latch the output of the VLC detector. If the VLC is hit in cache1, the power required to activate the VLC detector is saved. If not hit in cache1, the power and the cycle needed to access the cache are wasted. However, the cache power is much less than that of the VLC detector and the probability that the VLC is hit in the cache is as high as 0.8 for even a small-sized cache containing only eight short codewords. Therefore we can reduce the power on average. In addition, letting the next VLC go directly to LUT2, instead of to LUT1, can compensate for the cycle penalty caused by cache misses. This can be achieved by making the cache contain the short codewords of LUT1. We do not need to access LUT1, because if a codeword is not in the cache that satisfies the above property, it is guaranteed that the codeword is not in LUT1. Therefore, it is possible to save power without sacrificing performance.

In the proposed scheme, LUT1 and cache1 are accessed sequentially. However, we can envisage other configurations, because, as mentioned before, the output of the VLC detector is sufficient to cover two short codewords. One possible configuration would be possible by enlarging LUT1 to generate two short codewords, and the other realised by allowing LUT1 and cache1 to be accessed in parallel. Although these configurations are more useful in terms of throughput, the former results in a large-sized LUT and the latter leads to the cache being activated every cycle, resulting in a higher power consumption than that of the proposed scheme in our power simulation.

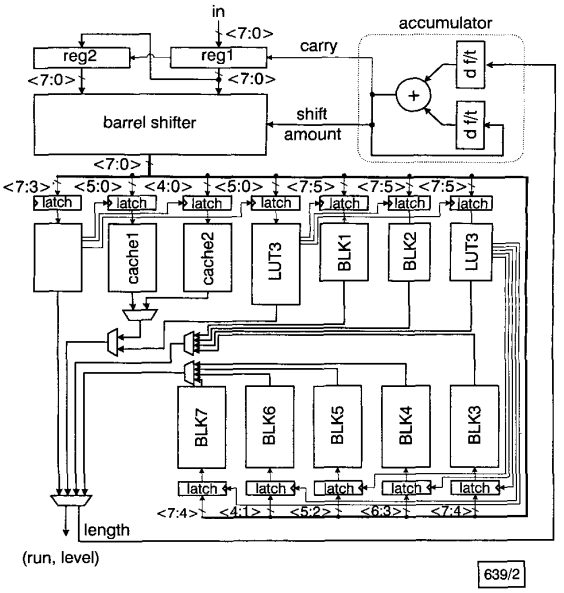

Fig. 2 *Block diagram of proposed low power VLD*

Implementation: To validate the proposed cache scheme in a practical design, we implemented a low-power VLD that has a similar structure to that of [3], except that the proposed cache is introduced in the structure, and the accumulator is modified to take into account the cache effect. As the accumulator in [3] has a latch at the output side of the adder, the adder is activated whenever its inputs are changed. This is unnecessary when we need to access the cache. For the purpose of preventing the unintended addition, two latches are placed at the input side of the adder.

The architecture of the VLD implemented is shown in Fig. 2, which has two caches separated to further reduce the cache power: cache1 and cache2. If the size of a short codeword found in LUT1 is 2 bits, cache1 is accessed. Cache2 is accessed for a 3 bit codeword. The other blocks such as LUT2, BLK1, and BLK2 have the same function as those of the VLD structure in [3].

Table 1: Performance and power evaluation

	Power consumption	Throughput	Energy for decoding 10 kbytes
	μW/MHz	bit/cycle	μJ
Previous VLD [3]	114.52	3.148	2.911
Proposed VLD	82.66	3.530	1.873

The power consumption of the proposed VLD was compared to that of the previous VLD [3] known as the best low-power VLD structure. The power simulation results are summarised in Table 1. In addition to the higher throughput, a ~30% power reduction is achieved by employing the proposed cache scheme.

Conclusion: In this Letter, a low-power VLD has been presented based on the statistics of two successive codewords. It employs a small LUT working as a fixed cache to reduce the number of activations of a VLC detector which consumes a large amount of power. The overall power is significantly reduced at the expense of a small increase in circuit overhead. Intensive simulation results show that use of the proposed scheme can reduce energy by 35% on average without sacrificing throughput.

14 January 2000
Electronics Letters Online No: 20000364
DOI: 10.1049/el:20000364

Sung-won Lee and In-Cheol Park (*Department of Electrical Engineering, Korea Advanced Institute of Science and Technology, 373-1, Kusong-dong, Yusung-gu, Taejon, 305-701, Korea*)

References

1 SUN, M.T., and LEI, S.M.: 'A parallel variable-length-code decoder for advanced television applications'. Proc. 3rd Int. Workshop on HDTV, Torino, Italy, August 1989
2 CHOI, S.B., and LEE, M.H.: 'High speed pattern matching for a fast Huffman decoder', *IEEE Trans. Consumer Electron.*, 1995, **41**, pp. 97–103
3 CHO, S.H., XANTHOPOULOS, T., and CHANDRAKASAN, A.P.: 'An ultra low power variable length decoder for MPEG-2 based on nonuniform fine-grain table partitioning', *IEEE Trans. VLSI Syst.*, 1999, **7**, (2), pp. 249–257
4 LIN, C.H., and JEN, C.W.: 'Low power parallel Huffman decoding', *Electron. Lett.*, 1998, **34**, (3), pp. 240–241

Optimisation of baseband modulation scheme for millimetre-wave fibre-radio systems

C. Lim, A. Nirmalathas, D. Novak and R. Waterhouse

The optimisation of a modulation scheme for simultaneous transmission of baseband digital data and remote local oscillator (LO) signal delivery for application in a millimetre-wave fibre-radio system is presented. An analytical model is developed to investigate the performance of the modulation scheme. Good agreement with measurements is observed and it is found that a range of operating parameters exist which enable optimal system performance.

Introduction: Millimetre-wave (mm-wave) fibre-wireless networks have been proposed for the provision of future broadband services with data rates > 1Gbit/s [1, 2]. Possible architectures for transportation of these radio signals over fibre include: RF over fibre where the signal is distributed to and from the base station (BS) as a mm-wave frequency [2]; intermediate frequency (IF) over fibre using lower frequency subcarriers with frequency up-conversion at the BS [3]; and baseband transmission where the data is also up-converted to the required radio frequency at the remote site [4]. RF over fibre has the advantage of simplifying the BS design, although fibre chromatic dispersion can severely limit the performance of such links [5].

Previous investigations of mm-wave fibre-radio systems have focused on RF and IF signal transportation over fibre; however, a detailed investigation of baseband data transport schemes for these applications has yet to be carried out. Recently, we proposed a novel modulation scheme which incorporates simultaneous baseband data transmission and dispersion tolerant remote local oscillator (LO) signal delivery using a single dual-electrode Mach-Zehnder modulator (MZM) [4]. We successfully demonstrated the application of the modulation scheme in a full-duplex broadband mm-wave fibre-radio system operating at 34.8–37.5GHz. In this Letter, we develop an analytical model to investigate the sensitivity of the baseband modulation scheme to the MZM operating parameters to establish optimum system performance.

Modulation scheme: Fig. 1 shows the experimental setup of the mm-wave fibre-radio system downlink incorporating the modulation scheme for baseband data transmission and remote delivery of the LO [4]. The dual-electrode MZM is biased at quadrature and modulates the output of a distributed feedback laser (DFB). A baseband digital data stream (622Mbit/s) and an RF signal with frequency, $f_{LO}/2$ = 18.5GHz (where f_{LO} is the required LO frequency) are applied separately to the MZM arms. At the output of the modulator, the optical spectrum consists of the modulated optical carrier and the RF modulating sidebands spaced at $f_{LO}/2$ from the carrier. A fibre-grating (FG) at the output of the modulator suppresses second-order sidebands due to the MZM nonlinearity. Upon detection of the optical signal by a high speed photodetector (PD) at the BS, the RF spectrum consists of the recovered baseband data and RF signals at $f_{LO}/2$ and f_{LO}. The unwanted component at $f_{LO}/2$ is rejected using a bandpass filter (BPF) centred at f_{LO}. The frequency component at f_{LO} is a single RF tone generated from the beating between the two optical sidebands and is the required LO signal for mm-wave frequency up- and down-conversion of the down- and uplink baseband data streams.

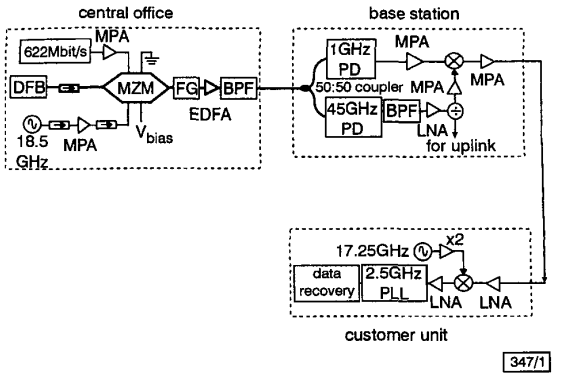

Fig. 1 *Experimental setup of millimetre-wave fibre-radio downunk incorporating baseband modulation scheme*

——— optical
——— electrical
PLL: phase locked loop, MPA: medium power amplifier, LNA: low noise amplifier, EDFA: erbium-doped fibre amplifier

Optimisation of modulation scheme: The operation of the baseband modulation scheme will depend on the input parameters to the MZM, namely the input RF power of the signal at $f_{LO}/2$, the input digital data amplitude and the modulator DC bias voltage. An analytical model of the baseband modulation scheme was developed to enable the optimal link performance to be investigated and to provide a comparison with the experimental results. In the analysis the output electric field from the dual-electrode MZM is modelled using the equation

$$E_O(t) = \frac{E_i e^{j\omega_c t}}{2}\left(e^{j\frac{\pi}{2}V_1(t)} - e^{j\frac{\pi}{2}V_2(t)}\right) \quad (1)$$

where $E_i e^{j\omega_c t}$ is the input optical field with optical frequency ω_c and amplitude E_i. $V_1(t)$ and $V_2(t)$ represent the modulating baseband data and RF analogue signal, respectively, normalised with respect to the MZM switching voltage V_π:

$$V_1(t) = \frac{1}{V_\pi}[a_1 s_1(t)] \quad \text{and}$$
$$V_2(t) = \frac{1}{V_\pi}[a_2 s_2(t) + a_3 s_3(t) + V_b] \quad (2)$$

In eqn. 2:

$$s_1(t) = \{-1, 1\} \qquad s_2(t) = \cos\left(2\pi\frac{f_{LO}}{2}t\right)$$
$$s_3(t) = \cos\left(4\pi\frac{f_{LO}}{2}t\right) \quad (3)$$

where a_n represent the signal amplitudes and V_b is the DC bias voltage of the MZM. Since the MZM requires high power drive electronics (> 23dBm), second-order harmonics $f_{LO}/2$ are also present in the input applied signal ($a_3 s_3(t)$ in eqn. 2).

The model also incorporates the gain or loss of the optical and electrical devices in the link shown in Fig. 1. The detected RF power after the PD at the BS can be calculated from the photodetector current. Fig. 2 shows the measured and calculated detected RF powers at both f_{LO} (37GHz) and $f_{LO}/2$ (18.5GHz) as a function of the MZM DC bias voltage, with no baseband data applied. The model parameters, a_1, a_2 and a_3, were set to the experimental values: 0, 2.5 and 0.9V, respectively. The theoretical results show good agreement with measurements for both signal frequencies investigated, confirming the accuracy of the model. Fig. 2 also